Enhancing carbon dots fluorescence via plasmonic resonance energy transfer

A. Sciortino [a b], A. Panniello [c], G. Minervini [c d], N. Mauro [e], G. Giammona [e], G. Buscarino [a b], M. Cannas [a], M. Striccoli [c], F. Messina [a b]

[a] Dipartimento di Fisica e Chimica – Emilio Segré, Università degli Studi di Palermo, Via Archirafi 36, Palermo 90123, Italy

[b] ATeN Center – Università degli Studi di Palermo, Palermo Italy

[c] CNR-IPCF-Bari Division, Via Orabona 4, Bari 70126, Italy

[d] Polytechnic University of Bari, Via Edoardo Orabona, 4, Bari BA 70126, Italy

[e] Dipartimento di Scienze e Tecnologie Biologiche, Chimiche e Farmaceutiche, Università degli Studi di Palermo, Via Archirafi 32, Palermo 90123, Italy

Corresponding authors:

A. Sciortino (alice.sciortino02@unipa.it); F. Messina (fabrizio.messina@unipa.it)

Highlights

- Enhancement of red emission of carbon nanodots by plasmonic resonance energy transfer.
- Ultrafast spectroscopic investigation on plasmonic resonance energy transfer.
- Spectroscopic study of carbon nanodots- Gold nanoparticle composite by ultrafast pump probe measurements.

Keywords

Plasmonic nanoparticles; Carbon nanodots; Energy transfer; Fluorescence

1. Introduction

Zero-dimensional carbon nanomaterials are a center of interest in nanoscience [1,2]. In particular, luminescent carbon nanodots (CDs) are being intensely investigated because of their light absorption-emission in the visible range [3-5], which is accompanied by several other interesting properties as the ease of synthesis [6,7], non-toxicity [8], and the simplicity of coupling with other nanomaterials [9,10]. With their highly tunable optical response, CDs offer a broad palette of light absorbers and emitters which are useful for several applications and can be integrated in many functional nanocomposites.

One of the most demanding challenges regarding carbon nanoparticles (NPs) is the synthesis of CDs displaying an intense orange-red emission. In fact, obtaining efficient CD emissions at long-

wavelengths is crucial for bioimaging [11,12], to reduce overlap with tissue autofluorescence and to match the biological transparency window. Furthermore, the poor performance of red-emitting CDs is the critical obstacle to fully use them in light-emitting devices [13]. Recently, many authors tried to synthesize red-emitting CDs, for example by carbonization of molecular precursors [14-16] or polymers [17], but typical emission quantum yields (QY) exceed 5% only in few cases [13], [18-22]. Here we explore an entirely different route to enhance CD emission, based on their coupling to plasmonic NPs.

Metal NPs as gold and silver display broadly tunable optical properties dominated by surface plasmon resonances (SPRs). These appear as characteristic optical absorption (OA) features with very high cross sections, whose peaks dramatically depend on the size, shape, chemical identity of the specific NPs and the environment they are exposed to [23]. The SPR is a coherent oscillation of conduction electrons coupled with the external electromagnetic field. Such an excited state stores a large quantity of energy which can be harnessed for many goals. Indeed, an intense research focuses on the fundamental interactions of plasmonic NPs with nearby chromophores, and how they can be exploited in photonics [24]. Plasmonic NPs can behave as nanoantennas undergoing bi-directional energy exchanges with proximate chromophores [25,26]. While SPR excitation can be transferred to the chromophore via an energy transfer, an excited fluorophore can also couple to SPRs leading to an enhancement of the radiative rate through the Purcell effect [27,28]. However, the coupling of SPR with emitting fluorophores can also produce an emission quenching via an electron transfer to the metal [29]. For example, the complex interplay of these phenomena lies at the root of surface-enhanced Raman scattering [30,31]. where metal NPs are used to increase a Raman signal and simultaneously decrease the fluorescence background.

The possibility of capitalizing on plasmonic NPs to control the optical response of CDs has only been explored by few recent works [32-35]. In particular fluorescence enhancement was demonstrated in the blue-green range, especially by coupling CDs to AgNPs, but the fundamental mechanism has not been completely unraveled [32-34]. Here we couple orange-emitting CDs with Au NPs to build nanohybrids in solution by playing with their interparticle distance. Thus we investigate the optical features of the nanohybrids when the two species are coupled by a direct electrostatic interaction, or when they are separated inserting a polymeric spacer on CD surface. Thereby, we demonstrate that the orange emission of the polymer modified CDs can be enhanced as much as fivefold when they interact with AuNPs. We also clarify the fundamental mechanism of such enhancement, as a coherent resonance energy transfer occurring in less than 70 femtoseconds (fs) from the metal nano-antenna to coupled CDs. The effectiveness and generality of our strategy makes it very promising for future optoelectronic applications of CDs.

2. Results and discussion

We synthesized CDs by a hydrothermal route described in a previous paper [11] and in the SI. As inferred by high-resolution transmission electron microscopy (HRTEM) and atomic force microscopy (AFM) measurements, the average size of these CDs is about 1.5 nm, while infrared (IR) absorption investigation and ζ potential measurements reveal that the surface is mainly functionalized by carboxylic groups displaying a negative charge of about −22 mV (Figs. 1 and S1). The OA and emission (PL) spectra of CDs in aqueous suspension are displayed in Fig. 1a. The OA shows a band at 540 nm, while the emission peaks at 620 nm with a QY≈4%. The as synthesized AuNPs have a size around 20 nm (Fig. S2) and have been specifically functionalized by a post synthetic treatment with CTAB to have a positive surface charge (ζ potential = +23 mV). Their OA spectrum (Fig. 1a) displays the SPR peak at 520 nm sitting on the tail due to 5s→6sp interband transitions, beginning above a 2.38 eV threshold [36].

Comparing CDs optical properties with the absorption spectrum of AuNPs highlights a good overlap of the plasmonic absorption to both the OA and PL of the CDs (Fig. 1a). This overlap paves the way to different types of photophysical interactions between AuNPs and CDs [37]. As a

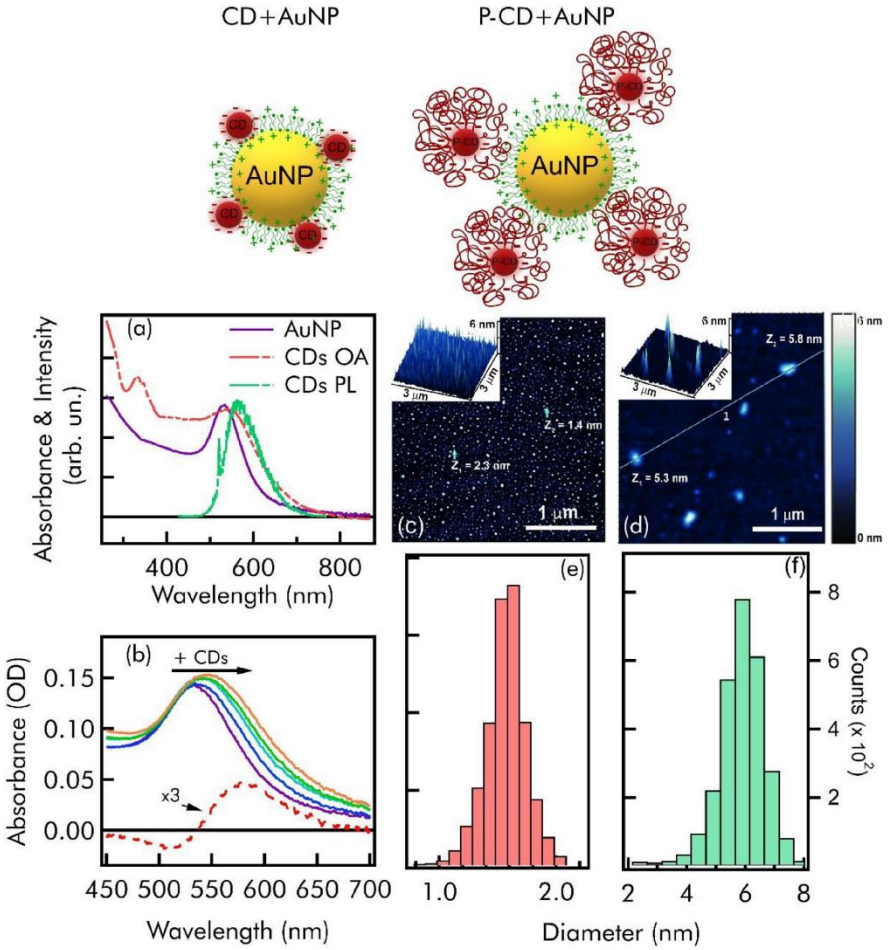

Fig. 1. Schematic representation of CDs-AuNP complexes when the CDs are in close contact to the gold NPs (left sketch) and when the CDs are separated from AuNP surface by the polymeric spacer (right sketch). (a) Absorption spectra of AuNPs (purple line) and of CDs (red line), both dispersed in water, and emission spectrum of CDs excited at 520 nm. (b) Absorption spectra of 2 nM AuNP water dispersion (purple line) after the addition of increasing amounts of CDs (from 24 to 130 µg/mL, see Table S1). The dotted red curve is the difference between the spectrum of bare AuNP dispersion and the spectrum of AuNPs with 24 µg/mL of carbon dots. AFM images of CDs (c) and P-CDs (d) on mica substrate, and the corresponding size distributions (e, f, respectively) extracted from AFM images.

consequence of our synthesis and functionalization protocols, CDs and AuNPs display opposite surface charges, which should induce their coupling through electrostatic interactions. In fact, the addition of minimal amounts of CDs to an AuNP 2 nM dispersion (Fig. 1b) leads to a measurable progressive redshift of the plasmonic peak, as shown by the derivative-like shape of the difference spectrum between bare AuNPs and AuNPs after the addition of 24 µg/mL of CDs. In fact, plasmonic resonances are very sensitive to environmental variations, as the dielectric constant of the media or the presence of molecules interacting at very close range [38]. Thus, this result clearly demonstrates an electrostatic interaction between Au NPs and CDs.

Once verified that AuNPs and CDs effectively interact in solution, we addressed how this interaction affects CD optical properties, by measuring the variations of CD emission as a function of AuNP concentration. As displayed in Figs. 2a and S3, the emission intensity undergoes a strong reduction in the presence of AuNPs without any changes of the lifetime (Fig. 2b). The latter observation indicates that the interaction responsible for quenching occurs on a sub-nanosecond scale. In the conditions of the experiment, fluorescence quenching is unsurprising and most likely a consequence of the photoinduced electron transfer from the HOMO of CDs (located at −3.9 eV [39])

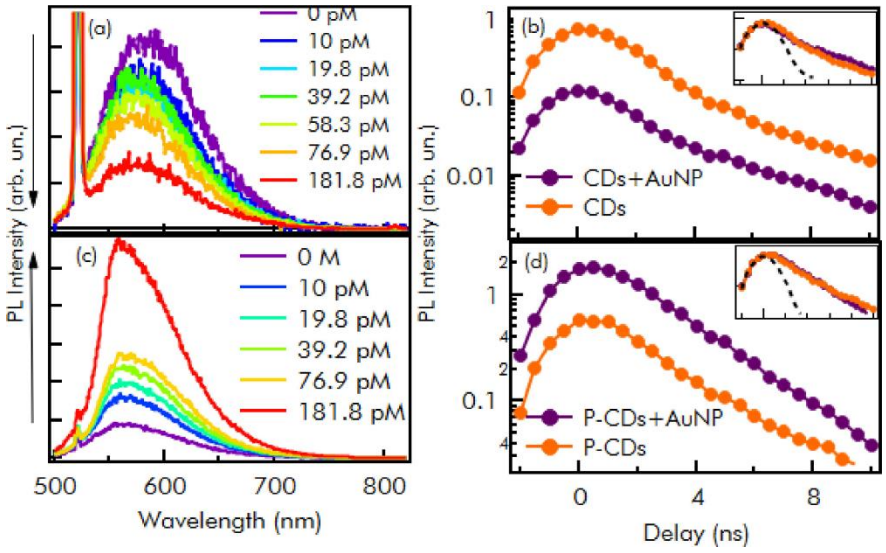

Fig. 2. (a) Emission spectra excited at 520 nm of CDs combined with different amounts of AuNPs. (b) Emission decay kinetics of CDs (orange line) and of CDs/AuNPs (purple line) excited at 520 nm. Inset: Normalized kinetics and instrumental response function (dashed line). (c) Emission spectra excited at 520 nm of P-CDs combined with different amount of AuNPs. (d) Emission decay kinetics of P-CDs (orange line) and of P-CDs/AuNPs (purple line) excited at 520 nm. Inset: Normalized kinetics and instrumental response function (dashed line).

to the Fermi level of Au NPs (−4.95 eV [40]) or an energy transfer from the CDs to the plasmonic nanoparticles. Considering the strong propensity of CDs to undergo to photoinduced electron transfer to coupled nanosystems [5,10], an ultrafast electron transfer seems to be more probable, as observed in other cases [9]. In addition, being an electron transfer a very short-range phenomenon with an effective range of a few angstroms [41], such a result strongly indicates the achievement of a close contact between AuNPs and CDs.

Therefore, one should be able to eliminate electron transfer by increasing the distance between CDs and AuNPs, so as to favor other types of interactions. Thus, we functionalized CD surface with polymeric PEG2000 chains, to be used as spacers between CDs and AuNPs within the nanohybrid. Details of the pegylation procedure are provided in the SI and in a previous publication [11]. The most important points are two: this procedure passivates the surface of dots without affecting their orange electronic transition, and the AFM diameter of pegylated-CDs (P-CDs) increases from 1.5 to 6 nm (Fig. 1). As found in other cases [42], the increase is significantly smaller than the length of extended PEG2000 chains, thus suggesting that P-CDs are covered by PEG chains rolled up on the CD surface in a 'mushroom' configuration [43,44], forming a layer about (6.0−1.5)/2 ≈ 1.75 nm thick. We found that the surface of P-CDs remains negatively charged (ζ potential = −12.6 mV), although the mean value is reduced with respect to bare CDs.

On these grounds, one can anticipate that P-CDs should still spontaneously couple with the positively charged AuNPs, while being now separated by ≈2 nm from their surfaces. Figs. 2c and S4 show the effect on P-CD emission upon the addition of increasing amounts of AuNPs. In striking contrast to Fig. 2a, we now see an increase of the PL intensity as a function of AuNP concentration. This effect occurs again without any changes in the emission lifetime (Fig. 2d) suggesting that the interaction responsible for the enhancement operates on a sub-nanosecond scale. In the explored range of AuNP concentration (from 0 to 180 pM) the emission increases by a factor of ≈ 6 corresponding to a final QY of 25%. This result clearly confirms the ability of AuNPs to enhance the emission efficiency of P-CDs, provided the two are separated by a polymeric spacer to eliminate the short-range quenching effect. Notably, the enhancement factor is most likely underestimated,

because not all P-CDs are expected to combine with the AuNPs, even if each Au NP is most likely surrounded by several P-CDs considering the large difference in size between the two.

To learn more about the enhancement mechanism, we measured photoluminescence excitation spectra (PLE) of P-CDs with and without AuNPs. Comparing the PLE spectra (Fig. S5b) demonstrates that the increment of orange emission stems from the plasmonic resonance. In fact, in the PLE of P-CD/AuNPs nanohybrids we observe an emerging contribution matching the spectral range (2.2–2.8 eV) of AuNP plasmonic resonance. The dramatic PL enhancement without any lifetime changes (Fig. 2c–d) and this variation in the PLE spectrum suggest the involvement of a near-field enhancement effect (NFE) [45] by which an incident electromagnetic field is converted in light intensity concentrated near the plasmonic particle surface. In proximity of AuNPs, CDs experience a strongly enhanced field at the excitation wavelength, increasing their excitation probability and, in turn, the emission intensity. Indeed, calculations predict a significant NFE within a distance of about 1/10 of the AuNP diameter [45]. The estimated separation distance of 1.75 nm between P-CDs and AuNPs clearly verifies this condition. Thus, the amplification observed in Fig. 2c ultimately stems from enhancing the excitation cross section of CDs through AuNPs. In contrast, the lack of lifetime changes (Fig. 2d) rules out any change of the radiative rate (Purcell effect) in proximity of the metal NP surface, which could also contribute to amplify the fluorescence [27]. What should be stressed here is that while the Purcell effect can only enhance the emission from a low starting QY, the amplification factor provided by NFE should still be ≈ 5 for any initial QY of the CDs. Thus, our method is very general and could be combined to any other strategy capable of enhancing the emission by chemical engineering, leading to a multiplicative effect.

The emerging contribution to the PLE induced by AuNPs (Fig. S5b) represents the excitation profile of the NFE effect. Further studies will be needed to model in detail the spectral shape of this function. Interestingly, it does not perfectly reproduce the plasmonic band of AuNPs, which is broader and slightly blue shifted. On one hand, this is not surprising considering that we are looking at the excitation spectrum of the nanohybrids, which can somehow differ from the absorption spectrum of the plasmonic NP alone. Furthermore, we observe that the size range for effective NFE is probably narrower than the overall polydispersity broadening the plasmonic absorption, and that for AuNPs it has been demonstrated that the maximum of NFE efficiency is redshifted from the spectral maximum of the extinction coefficient of NPs having the same diameter [45].

Describing AuNP/P-CD interactions in terms of NFE provides a useful macroscopic picture founded on the peculiar distribution of the classical electric field in proximity of the AuNPs. However, such a picture is incomplete and hides microscopic details on the dynamics of the photophysical interaction between the two nanomaterials. Thus, we performed femtosecond pump-probe (TA) measurements to further investigate this point. In Fig. 3a we show the TA signal of a 2 nM dispersion of bare AuNPs (that is, without P-CDs) excited with pulses at 540 nm (2.3 eV) having 20 nJ energy and 70 fs duration, plotted as a function of delay from photoexcitation. The signal displays a strong negative component close to the plasmonic peak, and positive wings in both tails. A time trace at the negative peak shows that the signal rises in τ_1 = 500 fs, and then decays with a bi-exponential behavior: τ_2 = 3 ps, τ_3 = 100 ps (fitting curves in Fig. S6). The experiment was also repeated with 600 nm (2.06 eV) excitation, which is below the 5s→6sp interband transition threshold (2.38 eV), in order to check for effects due to interband excitation. A comparison between normalized TA signals excited at 600 and at 540 nm in Fig. S7 shows that the signals are perfectly identical. This demonstrates that the effects of interband excitation in our conditions are negligible.

The shape and dynamics of our TA signal is quite common for metal NPs and usually described with the so-called “two temperatures” model [23,46]. In short, the coherent plasmonic oscillation generated by photoexcitation dephases very quickly (a few tens of fs, not observable here)

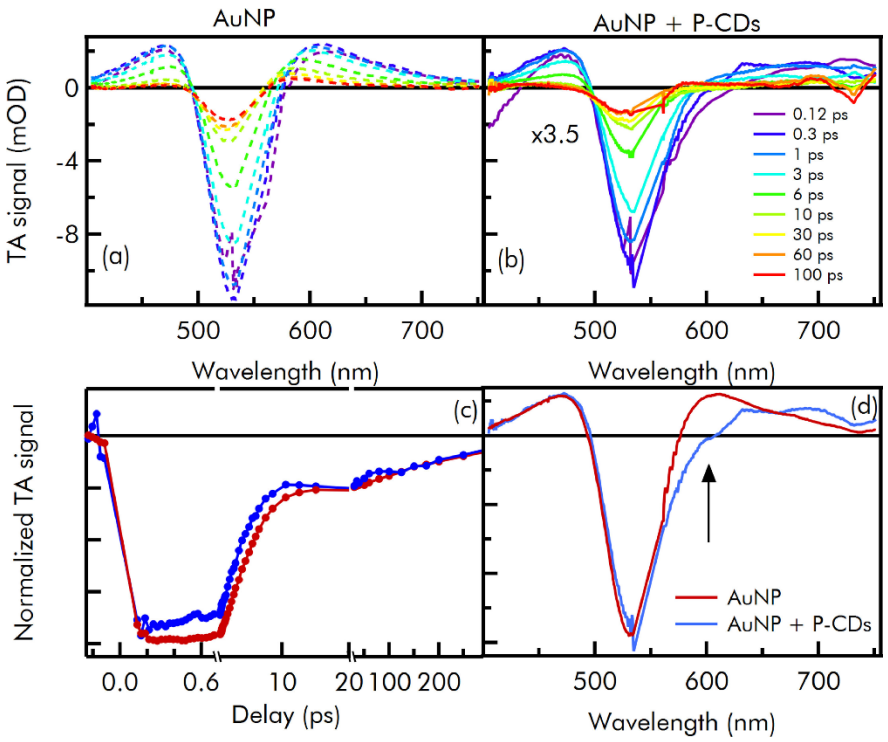

Fig. 3. (a) Transient absorption spectra of AuNPs at different delays from the 540-pump excitation. (b) Transient absorption spectra of AuNPs/P-CDs at different delays from the pump excitation. (c) Kinetics of TA signal at 515 nm of AuNPs without (red line) and with P-CDs (blue line) (d) Normalized TA spectra of AuNPs without (red line) and with P-CDs (blue line) at 300 fs.

after which the NP fully thermalizes through a sequence of three mechanisms [46]: electron-electron scattering (τ_1), electron-phonon scattering (τ_2), and finally (τ_3) the outward dissipation of stored energy to the solvent [46]. Importantly, the specific time scales are known to depend on the number of excitations hosted per NP: because electron-electron and electron-phonon scattering are many-body interactions, their timescales become faster when the number of excitations within the NP becomes lower, as can be observed for example when reducing excitation intensity [47].

After studying the bare AuNPs, the TA experiments were then repeated on the AuNP dispersion after the addition of an aliquot of P-CDs. The final dispersion has a concentration of 200 µg/L of P-CDs and 2 nM of Au NPs. Addition of P-CDs was performed in situ in order to compare the signal in perfectly identical excitation and detection conditions. Besides, the added P-CDs are so diluted in concentration that their own TA signal is undetectable in the absence of AuNPs, as we verified in a control experiment. Therefore, we focus on the changes of the TA signal of AuNPs induced by P-CDs. In the presence of P-CDs, the recorded signal from AuNPs displays about 3.5 times lower intensity already at the earliest delay time of the experiment (Fig. 3b) implying that their interaction with P-CDs happens below our time resolution of 70 fs. Such a strong decrease of the TA signal of AuNPs indicates their extremely fast de-excitation by transfer of energy stored in plasmonic oscillations to P-CDs. This process occurs quasi-instantaneously (< 70 fs), that is within the temporal interval during which the excited plasmon has not dephased yet. While the shape of the signals with or without P-CDs is similar in the central and blue region, important differences are observed in the orange spectral region (Fig. 3d). In particular, the addition of P-CDs generates an additional negative contribution to the TA signal around 600–620 nm (indicated by the arrows). This negative band is equally observed when exciting at 540 and 600 nm (Fig. S7d). It can be attributed to an additional induced fluorescence signal of P-CDs (detected in TA as a stimulated emission), which appears as the outcome of the energy transfer from AuNPs. Finally, comparing normalized temporal kinetics (see Figs. 3c and S6), it is also evident that the presence of P-CDs alters the relaxation time scales.

In particular, the electron-phonon relaxation time scale τ2 becomes shorter (from 3 to 1.5 ps) and the fastest electron-electron τ1 relaxation disappears, probably becoming shorter than our time resolution. Only the longest lifetime (τ3 = 100 ps) remains unaltered. Very similar changes are obtained exciting the complexes at 600 nm (Fig. S8). This shortening of the relaxation times is a direct consequence of the reduced number of excitations in the AuNPs, and thus it conclusively confirms the successful energy transfer to P-CDs.

Overall, these data demonstrate an energy transfer from the AuNPs to the coupled P-CDs occurring in less than 70 fs through a coherent mechanism. These are the fingerprints of what is called a plasmon resonance energy transfer (PRET) from the AuNPs to the P-CDs. PRET is a characteristic form of energy transfer from plasmonic nanosystems, in which the coherent plasmon state acts as an energy donor towards an acceptor, whenever a spectral overlap exists between the two absorption profiles (Fig. 1a). As found here, PRET occurs within an extremely short time scale which must compete with the decoherence time of the plasmon oscillation. Thus, we can conclude that PRET is the fundamental dynamical pathway through which AuNPs increase the excitation efficiency of P-CDs in the nanohybrids and, in turn, their fluorescence intensity. Interestingly, a previous work on CDs-Ag reports a similar degree of fluorescence enhancement to our own [33], but observed which a much large inter-particles distance (15 nm) suggesting a substantially different interaction mechanism.

In conclusion, we explored the use of plasmonics to boost the optical response of CDs in the orange region, and established a strategy to enhance their emission efficiency, at least by a factor of five, by coupling them to AuNPs. Experimental evidence shows that the enhancement stems from a coherent energy transfer from the plasmonic AuNP state to nearby P-CDs, occurring within 70 fs from photo-excitation, thus contributing to the fundamental understanding of photonic control through plasmonic phenomena. From a macroscopic viewpoint, this is equivalent to a near-field effect enhancing the absorption probability of CDs, hence in turn their fluorescence. Our approach only requires an overlap between the SPR resonance of AuNPs and the absorption band of CDs, and their stable electrostatic self-assembly in a nanohybrid through a suitable spacer. Therefore, it should be very general and transferrable virtually to any type of CDs absorbing in this region. Once this method is refined by fine tuning AuNP-CD spacing, and combined to other strategies capable of increasing the intrinsic QY of the dots, one should ultimately be able to obtain CD-AuNP nanohybrids displaying extremely large emission efficiencies in this spectral region. Thereby, this is a very promising pathway for using these hybrid nanomaterials in a wide range of applications.

Acknowledgement

The authors thank the Italian Ministry of University and Research (MUR) for funding received through project PRIN2017 “CANDL2”, grant number 2017W75RAE.

References

1. Ragazzon, G.; Cadranel, A.; Ushakova, E. V.; Wang, Y. C.; Guldi, D. M.; Rogach, A. L.; Kotov, N. A.; Prato, M., *Chem* **2021,** *7* (3), 606-628.
2. Zhu, S. J.; Song, Y. B.; Zhao, X. H.; Shao, J. R.; Zhang, J. H.; Yang, B., *Nano Research* **2015,** *8* (2), 355-381.
3. Mintz, K. J.; Bartoli, M.; Rovere, M.; Zhou, Y. Q.; Hettiarachchi, S. D.; Paudyal, S.; Chen, J. Y.; Domena, J. B.; Liyanage, P. Y.; Sampson, R.; Khadka, D.; Pandey, R. R.; Huang, S. X.; Chusuei, C. C.; Tagliaferro, A.; Leblanc, R. M., *Carbon* **2021,** *173*, 433-447.
4. Kang, Z. H.; Lee, S. T., *Nanoscale* **2019,** *11* (41), 19214-19224.

5. Sciortino, A.; Cannizzo, A.; Messina, F., *C-Journal of Carbon Research* **2018,** *4* (4).
6. Wang, J. Y.; Zhu, Y. H.; Wang, L., *Chemical Record* **2019,** *19* (10), 2083-2094.
7. de Medeiros, T. V.; Manioudakis, J.; Noun, F.; Macairan, J. R.; Victoria, F.; Naccache, R., *Journal of Materials Chemistry C* **2019,** *7* (24), 7175-7195.
8. Shi, X. B.; Wei, W.; Fu, Z. D.; Gao, W. L.; Zhang, C. Y.; Zhao, Q.; Dene, F. M.; Lu, X. Y., *Talanta* **2019,** *194*, 809-821.
9. Madonia, A.; Martin-Sabi, M.; Sciortino, A.; Agnello, S.; Cannas, M.; Ammar, S.; Messina, F.; Schaming, D., *Journal of Physical Chemistry Letters* **2020,** *11* (11), 4379-4384.
10. Pan, N. Y.; Okonjo, P. A.; Wang, P.; Tang, Y. G.; Sun, Y. P.; Yang, L. J., *Chemical Physics Letters* **2020,** *743*.
11. Scialabba, C.; Sciortino, A.; Messina, F.; Buscarino, G.; Cannas, M.; Roscigno, G.; Condorelli, G.; Cavallaro, G.; Giammona, G.; Mauro, N., *Acs Applied Materials & Interfaces* **2019,** *11* (22), 19854-19866.
12. Ji, C. Y.; Zhou, Y. Q.; Leblanc, R. M.; Peng, Z. L., *Acs Sensors* **2020,** *5* (9), 2724-2741.
13. Yuan, F. L.; Yuan, T.; Sui, L. Z.; Wang, Z. B.; Xi, Z. F.; Li, Y. C.; Li, X. H.; Fan, L. Z.; Tan, Z. A.; Chen, A. M.; Jin, M. X.; Yang, S. H., *Nature Communications* **2018,** *9*, 11.
14. Hola, K.; Sudolska, M.; Kalytchuk, S.; Nachtigallova, D.; Rogach, A. L.; Otyepka, M.; Zboril, R., *Acs Nano* **2017,** *11* (12), 12402-12410.
15. Song, Y.; Zhu, C. Z.; Song, J. H.; Li, H.; Du, D.; Lin, Y. H., *Acs Applied Materials & Interfaces* **2017,** *9* (8), 7399-7405.
16. Liu, Y. H.; Duan, W. X.; Song, W.; Liu, J. J.; Ren, C. L.; Wu, J.; Liu, D.; Chen, H. L., *Acs Applied Materials & Interfaces* **2017,** *9* (14), 12663-12672.
17. Ge, J. C.; Jia, Q. Y.; Liu, W. M.; Guo, L.; Liu, Q. Y.; Lan, M. H.; Zhang, H. Y.; Meng, X. M.; Wang, P. F., *Advanced Materials* **2015,** *27* (28), 4169-4177.
18. Jiang, K.; Sun, S.; Zhang, L.; Lu, Y.; Wu, A. G.; Cai, C. Z.; Lin, H. W., *Angewandte Chemie-International Edition* **2015,** *54* (18), 5360-5363.
19. Miao, X. A.; Yan, X. L.; Qu, D.; Li, D. B.; Tao, F. F.; Sun, Z. C., *Acs Applied Materials & Interfaces* **2017,** *9* (22), 18549-18556.
20. Ding, H.; Wei, J. S.; Zhong, N.; Gao, Q. Y.; Xiong, H. M., *Langmuir* **2017,** *33* (44), 12635-12642.
21. Ghosh, S.; Ali, H.; Jana, N. R., *Acs Sustainable Chemistry & Engineering* **2019,** *7* (14), 12629-12637.
22. Zhang, M. R.; Su, R. G.; Zhong, J.; Fei, L.; Cai, W.; Guan, Q. W.; Li, W. J.; Li, N.; Chen, Y. S.; Cai, L. L.; Xu, Q., *Nano Research* **2019,** *12* (4), 815-821.
23. Zhang, Y. C.; He, S.; Guo, W. X.; Hu, Y.; Huang, J. W.; Mulcahy, J. R.; Wei, W. D., *Chemical Reviews* **2018,** *118* (6), 2927-2954.
24. Navarro, J. R. G.; Lerouge, F., *Nanophotonics* **2017,** *6* (1), 71-92.
25. Giannini, V.; Fernandez-Dominguez, A. I.; Heck, S. C.; Maier, S. A., *Chemical Reviews* **2011,** *111* (6), 3888-3912.
26. Li, K.; Hogan, N. J.; Kale, M. J.; Halas, N. J.; Nordlander, P.; Christopher, P., *Nano Letters* **2017,** *17* (6), 3710-3717.
27. Luo, Y.; Ahmadi, E. D.; Shayan, K.; Ma, Y. C.; Mistry, K. S.; Zhang, C. J.; Hone, J.; Blackburn, J. L.; Strauf, S., *Nature Communications* **2017,** *8*.
28. Eliseev, S. P.; Kurochkin, N. S.; Vergeles, S. S.; Sychev, V. V.; Chubich, D. A.; Argyrakis, P.; Kolymagin, D. A.; Vitukhnovskii, A. G., *Jetp Letters* **2017,** *105* (9), 577-581.
29. Nikoobakht, B.; Burda, C.; Braun, M.; Hun, M.; El-Sayed, M. A., *Photochemistry and Photobiology* **2002,** *75* (6), 591-597.
30. Amato, F.; Micciche, C.; Cannas, M.; Gelardi, F. M.; Pignataro, B.; Vigni, M. L.; Agnello, S., *European Physical Journal Plus* **2018,** *133* (2).
31. Kolataj, K.; Krajczewski, J.; Kudelski, A., *Environmental Chemistry Letters* **2020,** *18* (3), 529-542.
32. Jana, J.; Aditya, T.; Ganguly, M.; Mehetor, S. K.; Pal, T., *Spectrochimica Acta Part a-Molecular and Biomolecular Spectroscopy* **2018,** *188*, 551-560.
33. Yuan, K.; Qin, R. H.; Yu, J. J.; Li, X.; Li, L. L.; Yang, X. J.; Yu, X. F.; Lu, Z. M.; Zhang, X. H.; Liu, H., *Applied Surface Science* **2020,** *502*.

34. Emam, A. N.; Mostafa, A. A.; Mohamed, M. B.; Gadallah, A. S.; El-Kemary, M., *Journal of Luminescence* **2018,** *200*, 287-297.
35. Efremushkin, L.; Bhunia, S. K.; Jelinek, R.; Salomon, A., *Journal of Physical Chemistry Letters* **2017,** *8* (24), 6080-6085.
36. Zhang, X. P.; Huang, C. Y.; Wang, M.; Huang, P.; He, X. K.; Wei, Z. Y., *Scientific Reports* **2018,** *8*.
37. Li, J. T.; Cushing, S. K.; Meng, F. K.; Senty, T. R.; Bristow, A. D.; Wu, N. Q., *Nature Photonics* **2015,** *9* (9), 601-+.
38. Derkachova, A.; Kolwas, K.; Demchenko, I., *Plasmonics* **2016,** *11* (3), 941-951.
39. Sciortino, A.; Ferrante, F.; Mauro, N.; Buscarino, G.; Sciortino, L.; Giammona, G.; Cannas, M.; Duca, D.; Messina, F., *Carbon* **2021,** *173*, 454-461.
40. Sandeep, K.; Manoj, B.; Thomas, K. G., *Journal of Chemical Physics* **2020,** *152* (4).
41. Tavernier, H. L.; Fayer, M. D., *Journal of Physical Chemistry B* **2000,** *104* (48), 11541-11550.
42. Liu, R. L.; Wu, D. Q.; Liu, S. H.; Koynov, K.; Knoll, W.; Li, Q., *Angewandte Chemie-International Edition* **2009,** *48* (25), 4598-4601.
43. Jokerst, J. V.; Lobovkina, T.; Zare, R. N.; Gambhir, S. S., *Nanomedicine* **2011,** *6* (4), 715-728.
44. Suk, J. S.; Xu, Q. G.; Kim, N.; Hanes, J.; Ensign, L. M., *Advanced Drug Delivery Reviews* **2016,** *99*, 28-51.
45. Bisker, G.; Yelin, D., *Journal of the Optical Society of America B-Optical Physics* **2012,** *29* (6), 1383-1393.
46. Brongersma, M. L.; Halas, N. J.; Nordlander, P., *Nature Nanotechnology* **2015,** *10* (1), 25-34.
47. Hodak, J.; Martini, I.; Hartland, G. V., *Chemical Physics Letters* **1998,** *284* (1-2), 135-141.